Indonesian Physical Review

Volume 5 Issue 1, January 2022
P-ISSN: 2615-1278, E-ISSN: 2614-7904

Review of Characteristics and Properties of Fe_2O_3/SiO_2 As Water Pollution Prevention

Balada Soerya[1], Jaya Edianta[1], Siti Lailaturofi'ah[1], Aniendita Ningtyas[1], Fitri Suryani Arsyad[1,*], Dedi Setiabudidaya[1] and Siti Sailah[1]

[1] *Department of Physics, Faculty of Mathematics and Natural Sciences, Sriwijaya University. E-mail: fitri_suryani@unsri.ac.id*

ARTICLE INFO

Article info:
Received: 12-12-2021
Revised: 01-02-2022
Accepted: 07-02-2022

Keywords:
Fe_2O_3; SiO_2; Water Pollution; Characteristics

How To Cite:
Balada, S., Jaya, E., Siti, L., Aniendita, N., Fitri, S., A., Dedi, S., Siti, S. Review of characteristics and Properties of Fe_2O_3/SiO_2 as Water Pollution Prevention (2022). Indonesian Physical Review, 5(1), 36-56.

DOI:
https://doi.org/10.29303/ipr.v5i1.131

ABSTRACT

The existence of water on earth is very abundant and has a vital role in the source of life for every living creature. In managing water resources, pollution is one of the issues world researchers face. This article reviews the characteristics and methods of synthesizing Fe_2O_3 and SiO_2 materials to prevent water pollution. The strategies administrated antecedently square measure vapor deposition, microemulsion, solvothermal, coprecipitation, sol-gel, and hydrothermal. The formation of fine quality nanoparticles with controlled size associate degreed size distribution square measure typically achieved by selecting an applicable solvent mixture and varied parameters like temperature, pressure, and time interval.

Introduction

The existence of water on earth is very abundant and has a vital role in the source of life for every living creature. In managing water resources, water pollution is one of the problems faced by world researchers [1]. The spread of pollutants such as pharmaceutical and private care products, poly and perfluoroalkyl substances, biocides, essential metals, dyes, radionuclides, plastics, nanoparticles, and pathogens square measure among the pollutants of major concern [2]. In addition, the release of heavy metal ions in water is of substantial concern because of their very harmful effects on human health [3]. Some vital metals such as copper (Cu), cadmium (Cd), zinc (Zn), lead (Pb), mercury (Hg), arsenic (As), silver (Ag), Cr (Cr), iron (Fe), and noble metal (Pt) will cause injury to ecosystems and organisms like aerobic damage,

endocrine disorders, and even death [4]. Universally, researchers use several methods in dealing with decontamination and wastewater, namely biological, physical, and chemical [5]. The benefits of science and technology also play an important role in addressing water quality, for example, using best management practices (BMPs) for hydrology, machine learning algorithms to improve water quality modeling and remote sensing techniques in monitoring water quality [6]. However, most modern remediation methodologies involve nanocatalysts, adsorption, absorption-reduction, and photocatalytic degradation processes. Nanocatalysts are widely used in water pollution control because they are easy to synthesize and environmentally friendly [7]. But on the other hand, applying adsorption materials is one of the best methods to remove various contaminants from water, including heavy metals [4]. Some of the benefits of surface assimilation applications, namely the area unit high absorption capability, energy-saving, and environmental friendliness [8]. Some heavy metals in the environment have been successfully analyzed and removed using several materials as shown in Table 1. Adsorption applications are promising because they are easily synthesized in conventional materials such as activated carbon and biomaterials. Synthesis of advanced materials such as silica and magnetite ferrite are attractive components of materials that can be applied as adsorption, photocatalysis, and degradation of harmful molecules or metals gift in water. By utilizing nanotechnology, the fabrication of silica and magnetite ferrite materials can increase the functionality of the material in eliminating water pollution, because it will increase the high expanse furthermore as glorious mass transfer. [9], [10]. Based on theory and an in-depth literature review, we are interested in discussing more silica and magnetite ferrite materials.

Table 1. Review characteristics and parameters for adsorbtion of some heavy metals

Heavy metals	**Characteristics**	**Material adsorbtion**	**Parameter optimum adsorbtion**			**Ref.**
			pH	T(^{0}C)	Q(mg/g)	
Pb(II) and Cd (III)	comes from industry, gasoline pipelines, and water distribution, with friction value for and Pb(II) ions is 0.1 mgL-1	Activated Carbon	5.5-6	56.8	9.30	[11]
Al (III) and Fe (III)	can come from gas purification as a result of the reaction. It is toxic and, when ingested, can cause diseases such as anorexia, Alzheimer's, convulsive crises, liver and kidney disorders.	Chitosan film	4.5	25	140.2	[12]
Cr (III)	Chromium compounds derived from modern chemical waste cause nausea, diarrhea, liver failure, dermatitis (eczema), internal bleeding (bleeding), and respiratory problems.	Bio-adsorbtion	5	30	218.5	[13]
As (III)	Arsenic (As) is a very toxic substance in the aquatic environment. In natural water, arsenic exists mostly in two oxidation states: As(III) and As(V). The dominant arsenic species in groundwater is As(III)	Cu_2FeO_4/ PMS	6.7	Room temp	63.9	[14]
Cu (II) and Zn (II)	Copper(II), zinc(II), and cobalt(II)n ions are some of the most common heavy metal ions in modern industries such as mining, metallurgy, battery production, and metal plating. These heavy metals can multiply in organisms	Impregnated materials	3.16	Room temp	440 mmol/kg and 32 mmol/kg	[15]

Development of Research on SiO_2 and Fe_2O_3 Materials

Seeing research development on advanced materials in water pollution, SiO_2 and Fe_2O_3/Fe_3O_4 materials are more interested in, and research on them always develops every year. The result of research on SiO_2 and Fe_2O_3 materials into several applications can be seen in Table 2. A study on SiO_2 states that SiO_2 has the characteristics of a high surface area that can increase the mechanical strength of material products by utilizing nanotechnology [10]. In photocatalyst immobilization applications, SiO_2 is widely used for the stability and dispersion of core particles [16]. Doping SiO_2 on advanced materials can benefit high mass transport values and better selectivity for target pollutants [9]. In addition, the silicon dioxide core will act as an electron trapping center which can reduce the recombination rate and contribute to a rise within the photocatalytic rate [17]. In addition, SiO_2 also attracts attention because of its cheap and practical nature in applying water pollutant adsorption. Research [18] succeeded in synthesizing SiO_2 nanoparticles as an effective adsorbent to remove active metal pollutants Cu^{2+} and NO^{3-}. SiO_2 has been investigated and combined with several other compounds such as graphite, TiO_2 Carbon, MnO, ZnO, Ag, Fe_2O_3, and Fe_3O_4. We are interested in the advantages of Fe_2O_3 compounds, which are easy to obtain and synthesize and are environmentally friendly. Fe_2O_3 nanoparticles will show sensible photocatalytic degradation activity against totally different waste organic pollutants below visible irradiation. [19].

Several previous studies have reported some of the advantages of combining SiO_2 with Fe_2O_3, Research [20] succeeded in synthesizing photocatalytic nanocomposites to degrade methylene blue pollution in water. The magnetic nanocomposites they prepared were well dispersed in aqueous solutions and quickly recovered for recycling in multiple cycles and preventing the secondary decay of treated water. These composites perform well in sunlight and have great potential for inclusion in existing water treatment systems due to their high efficiency and low energy requirements. Schematic of $Fe_3O_4@SiO_2@C_3N_4/TiO_2$ nanocomposite research results [16] Can utilize more photons from sunlight, thereby increasing the photocatalytic degradability of organic dyes, the principle finds potential applications in environmental remediation. Detailed characterization of SiO_2 catalyst of α-$Fe_2O_3@MnO_2$ decreased catalytic activity on metal leaching process to phase composition change and intermediate adsorption at the active site [21].

Table 2. The development of SiO_2 and Fe_2O_3 applications as advanced materials in overcoming water pollution

Material	Synthesis method	Pollutant targets	Application	Ref.
SiO_2/graphite nanocomposite	The Hummers technique through the chemical reaction of natural carbon powder	Pb (II) ions	Adsorbsi	[22][23]
nano γ -Fe_2O_3 based magnetic cationic hydrogel	solution polymerization	Acid Red 27 and Acid Orange 52	Removal of ionizable aromatic pollutants	[24]
$Fe_3O_4/SiO_2/TiO_2$	coprecipitation and sol-gel	methylene blue, ciprofloxacin, norfloxacin, and ibuprofen	Decontamination of polluted water	[25]

α-Fe_2O_3 nanoparticles	Green synthesis	anionic and cationic dyes and dicholor ophenols	photocatalytic to decontaminate polluted water with different organic pollutants	[19]
γ-Fe_2O_3/SiO_2/ C-TiO_2	coprecipitation and sol-gel	methylene blue	photocatalytic degradation of organic pollutants	[20]
α-Fe_2O_3 Nanoparticles	polymeric precursor and hydrothermal	Rhodamine B (RhB) and atrazine (ATZ)	decontamination of polluted water	[26]
Fe_2O_3/TiO_2 functionalized biochar	One-step pyrolisis	methylene blue	catalyst for dyes degradation	[27]
Fe_3O_4@SiO_2@g-C_3N_4/TiO_2 nanocomposite	Solvothermal and hydrothermal	Cationic and anionic dyes	adsorbsi	[16]
ZnO.SiO_2 Nanocomposite	co-precipitation	methyl orange dye	the photo-degradation of the dye component	[17]
SiO_2 Nanoparticles	simple extraction and precipitation method	Cu^{2+} and NO^{3-}	Adsorbsi	[18]
SiO_2 with γ-Fe_2O_3/MnO_2	Multistep and hydrothermal	Phenol	Singlet oxygen-dominated degradation	[21]

Development of SiO_2 and Fe_2O_3 Utama Main Ingredients

Silica and iron sand/magnetite materials attracted our attention because they are easily synthesized and can be quickly processed from natural materials found in nature. It is in line with the advantages of the Indonesian area, which has several locations and raw materials that can synthesize silica and ferrite materials. The silica (SiO_2) material has been successfully synthesized by the coprecipitation method using the essential ingredients of Lapindo mud extract in Sidoarjo with a purity level of 96.9 wt% [28]. Several other natural materials have also succeeded in acting as caps or the main ingredient in synthesizing materials, such as strawberry fruit extract as a capping agent for the synthesis of mesoporous Fe_3O_4@SiO_2-hydroxyapatite nanocomposite using sonochemical methods [29]. Biogenic silica from bamboo leaves was also successfully synthesized using the sol-gel method application of photocatalytic composites for degradation of methylene blue with a very good semiconductor energy bandgap [30]. Several other plants such as sugar palm peel, pineapple leaf, and orange peel are useful as the main raw material in the manufacture of silica material which has the potential for adsorption, photocatalysis, degradation, and [31], [32]. One study also reported that one of Indonesia's natural resources, namely, rice husks has the potential to synthesize SiO_2 with a high purity level of 99.258% with coprecipitation techniques [33].

On the other hand, iron or magnetite sand also has the same advantages as silica, which is easy to synthesize through the main ingredients found in nature. Several methods of green synthesis or hydrothermal have succeeded in using natural extract materials in producing quality iron and magnetite sand, such as Euphorbia peplus Linn leaf extract [34], Chromolaena odorata root [35], euphorbia cochinchinensis [36], dan Carum carvi L. Seeds Aqueous [37].

Analysis Study of SiO_2 and Fe_2O_3 Combination Synthesis Methods

Various strategies have been developed for the synthesis of iron oxide MNPs. It includes synthesis using vapor deposition, microemulsions, solvothermal conditions, and coprecipitation [38]. In the study conducted by Sobhanardakani et al., they were able to come through columnar structures while not employing a catalyst for the primary time through a plasma-enhanced chemical vapor deposition technique to manage the expansion direction of nanostructures at air mass and cold by reactive victimization species generated within the plasma. Then, they studied the potency of removal (RE) of Hg(II) and Cr(VI) ions on Fe_2O_3@SiO_2 skinny films as new adsorbents beneath varied experimental conditions. In reverse microemulsion, the coprecipitation method happens simultaneously with the condensation method of $Si(OR)_{4-x}(OH)_x$. Precipitation of $Fe(OH)_3$ affects the porous shell construction. Analysis of Hongbu Yu et al. stated that Au α-Fe_2O_3@SiO_2 core-shell NPs with adjustable size and composition were ready by microemulsion technique. The relevant characterizations showed that the introduced Fe_2O_3 not solely resulted in shut contact with the Au cluster and suppressed its growth throughout oxidization; however, it conjointly enlarged the consistency of the SiO_2 shell by influencing its condensation [39]. Solvothermal methods are generally used to synthesize metallic elements, metal oxide materials, polymer composites, and others in various forms, such as polycrystalline in the form of nanopowder, including single crystals. Based on the research of Nadar et al., high pressure during the preparation of the solvothermal method in an autoclave produces samples in the size of nanoparticles in the form of spheres dispersed in silica. Fe_2O_3 with spherical geometry has a particle size ranging from 10− 20 nm. each lattice in the FSWI and FSST samples having a width of 0.23 nm shows α-Fe_2O_3 associated with hkl (123) in the plane of the polymorphic phase. [40]. The properties of the core with double shell nanoparticles obtained by the sol-gel methodology and hardened at 600°C were investigated. Once heat treatment, the α-Fe_2O_3 part is made as a photocatalyst shell. The Fe_3O_4 phase (magnetic core) is changed to become incredibly crystalline, finally forming α-Fe_3O_4/SiO_2/α-Fe_2O_3 core-shell structure with higher stability and better magnetism. Power saturation price [41]. Table 3 explain about review of the combined synthesis method of SiO_2 and Fe_2O_3.

Table 3. Review of the combined synthesis method of SiO_2 and Fe_2O_3

Substitution	Methode of Synthesis	Review of Result	Ref.
Synthesis of Mesoporous α-Fe_2O_3 Nanoparticles by Non-ionic	Hydrothermal	mesoporous nanoparticles α -Fe_2O_3, exhibiting a slim pore size distribution and a twenty-node median pore size) were obtained.	[42]
preparation of SiO_2@Ni-Al layered double hydroxide composites	Hydrothermal	highlight the potential applications of the SiO_2@Ni–Al LDH composites in associate degree automotive business like shock absorbers, engine mounts, and clutches.	[43]
γ-Fe_2O_3@SiO_2@TiO_2 photocatalyst induced by magnetic dipole interactions	Solvothermal and Sol-Gel	The assembly demonstrates sensible photocatalytic activity and magnetic recyclability.	[44]
photochemical synthesis of Au nanodots on α-Fe_2O_3@Reduced graphene chemical compound nanocomposite	Hydrothermal	The excited state of pigment generates additional photoelectrons and contributes to reducing Au^{3+} ions to Au° metal nanodots on the surface of the α-Fe_2O_3@RGO hetero-nano structure.	[45]

electrochemical performance of TiO_2-Fe_2O_3 nanocomposite	Hydrothermal	The photo-decolorization study shows that the TiO_2-Fe_2O_3 nanocomposite may be a smart photocatalyst for the organic decolorization of Titan Yellow (TY) and acid-base indicator (MO).	[46]
A hydrophobic FeMn@Si catalyst increases olefins	Hydrothermal	The hydrophobic shell protects the iron carbide core from oxidation by water generated during FTS and shortens water retention on the catalyst surface, resisting the side reactions associated with water.	[47]
material properties of $SiO_2/TiO_2/Nb_2O_5$ by sol-gel synthesis method	Sol-gel	showed high metal oxide dispersion on the silica matrix and the absence of section segregation (SBET).	[48]
carbonyl sulfide and carbon disulfide over Fe_2O_3 cluster:	Hydrolysis	The experimental results showed that the Fe_2O_3 cluster increased the chemical action-reaction result.	[49]
Fe_2O_3@ MIL-101(Fe)/C derived from metalorganic frameworks	MOF (Metal-Organic Framework)	the stable reversible capability of Fe_2O_3@MIL-101(Fe)/C conductor is 710 $mAhg^{-1}$, and might be maintained at 662 mAhg−1 when two hundred cycles with the retention of 93.2%.	[50]
Fe_2O_3 modified TiO_2 prepared by atomic layer deposition	Atomic Layer Deposition (ALD)	four hundred cycles of Fe_2O_3-coated TiO_2 Photocatalyst (~2.6 nm) showed a superb degradation potency of 97.4% in ninety min, well on top of the performance of pure TiO_2 powder of solely 12.5%.	[51]

Hydrothermal Method

Based on the development of Fe_2O_3/SiO_2 research in terms of controlling water pollution, the synthesis method, one method that has succeeded in synthesizing Fe_2O_3/SiO_2 as a water pollution control material is the hydrothermal synthesis method with a good level of homogeneity without reducing the characteristics of the two materials [7]. Hydrothermal synthesis of α-Fe_2O_3 and SiO_2-based nanocatalysts to form carbon-carbon bonds has been successfully carried out by [52] and Zanthoxylum rhetsa fruit extract [7].

Hydrothermal synthesis has benefits over different ways like a comparatively low price, non-toxicity, environmentally friendly precursors, and straightforward procedures. The formation of excellent quality nanoparticles with controlled size and size distribution may be achieved by choosing an acceptable solvent mixture and numerous parameters like temperature, pressure, and time interval [53].

Based on the research of Gholamrezaei et al.[54], the hydrothermal approach was chosen because of its low Cost, high efficiency, and potential for mass production. Given the fact that the uniqueness of the nanostructure is highly dependent on the size, dimensions, and shape. Hydrothermal is a proprietary process for preparing nanostructures with specific and controlled shapes, whereas other techniques such as sol-gel and sonochemistry largely provide nanoparticle morphology. The hydrothermal method provides a suitable morphological orientation. Under different special conditions, for example, high temperature and pressure, this approach produces different shapes in situ and forms several morphologies as nanoparticles, nanorods and nanoplates are obtained. Our method for Ag2Te synthesis is very simple, low Cost, and can be improved by using non-toxic precursors and solvents (TeCl4 as Te precursor). The synthesized material will be further processed into a photodegradation application material for methyl orange solution. As a result, the lamp emits a mixture of UVA,

ranging from 320 to 400 nm and UVB with a wavelength of 290–320 nm, and emits radiation of 13.6 and 3.0 W, respectively; it is free of ozone and radiation is encapsulated into a quartz tube, which is adrift in a methyl orange solution located in the center of the reactor [54].

Pivert et al.,[55], prepared ZnO NanoWire material grown on civil engineering samples by a two-step hydrothermal method at 350°C for 30 minutes to remove residual water in its porous structure. Hydrothermally first, their samples were impregnated with buffer solution (C= 0.01 M) $Zn(Ac)^2$ (zinc acetate dihydrate, 99%, VWR) in absolute ethanol (99.9%, VWR). The impregnation (short duration) was repeated four times, followed by thermal annealing at 350°C for 30 min. Then, a second step consisted of hydrothermal growth of ZnONW Cunanan autoclave containing an aqueous mixture of 0.05M methenamine (HMTA, 99%, VWR) and 0.05 M $Zn(NO_3)^2$ (zinc nitrate hexahydrate, 98%, Sigma-Aldrich) at 90°C. C for 4 hours. This step is useful for removing hydroxide residues and increasing ZnO crystallinity which can be a photocatalytic material for purifying acid red 14, methylene blue, and methyl orange water [55]. Yongshan Ma et al's research results [56] successfully synthesized ternary composites using the hydrothermal synthesis method. With this method, the photoelectrochemical measurement results show that the photocurrent performance of the ternary composite photocatalyst is superior to that of binary composites or NH_2-PD_I, MoS_2, or pure TiO_2. NH_2-PD_I/TiO_2/MoS_2 exhibited excellent photocatalytic activity and high stability [56].

In research, Makarchuk [57] provides info on organic dyes' sorption capability and removal potency by saponite sorbents, magnetic liquids, and nanocomposites. MCS 2, 4, and 7 were the foremost effective sorbents. That is, the sorption capability of MCS with relevancy all dyes inflated with increasing magnetic iron-ore content from 2-7% by weight. However, modification of saponite by magnetic iron-ore in AN quantity of 100% by weight caused a decrease within the sorption properties of MCS 10. the info obtained area unit following the characteristics of the porous structure of the nanocomposite.

The removal potency of mineral inexperienced, Congo red, and Indigo carmine, as an example, by MCS 7 was 3, 6, and 2.5 times on top of that of the saponite clay. The relative MCS 7 absorptions of mineral inexperienced, Congo red, and Indigo carmine exceeded the iron ore surface assimilation values of 9, 3, and 3.5 times, severally (Table 4). Thus, a synergistic result was ascertained for the ready magnetic nanocomposite sorbent material [57].

Table 4.The ratio of Fe_3O_4 and SiO_2 materials [57].

Sorbent	Malachite Green		Congo red		Indigo carmine	
	at, mg/g	X, %	at, mg/g	X, %	at, mg/g	X, %
Saponite	105.7	26.4	30.7	10.2	62.1	20.7
MCS 2	159.1	39.8	73.0	24.3	110.3	36.8
MCS 4	283.2	70.8	126.9	42.3	124.1	41.4
MCS 7	324.5	81.1	176.9	59.0	148.3	49.4
MCS 10	86.8	21.7	46.1	15.4	51.7	17.2
Fe_3O_4	36.7	9.2	59.6	19.9	44.8	14.9

Table 5. Reporting Fe_2O_3 content as calculable by Energy Dispersive X-Ray visible radiation qualitative analysis (EDXRF) of Fe_2O_3/SiO_2 catalyst synthesized by three different strategies. The values measured samples altogether were found to be at intervals ±6% of the supposed Fe_2O_3 content of 15% by weight. It shows quantitative dispersion overall 3 cases. However, the dispersion properties of the active elements, particularly the physical and chemical properties

of the spread iron chemical compound supported by the adopted producing technique, may be understood from the results of more characterization [40].

Table 5.The ratio of Fe_2O_3 and SiO_2 materials [40].

Sample	Preparation Method	Sample Abbreviation (1000° C calcined)	Fe_2O_3 content* (wt,%)	N2-BET Surface Area (m2/g)	Average Pore Radius (Rp)# (nm)
SiO_2	Commercial	SiO_2	-	249.5	12.91
Fe_2O_3/SiO_2	Polyol	FSP	15.8	122.8	9.04
Fe_2O_3/SiO_2	Wet-impregnation	FSWI	14.9	126.3	12.26
Fe_2O_3/SiO_2	Solvothermal	FSST	14.5	74.7	11.88

The Nitrogen-BET expansion of the samples is shown in Table 5. The area of the empty SiO_2 BET decreased from ~249 m^2/g to ~125 m^2/g for the FSP and FSWI samples ~75 m^2/g for the FSST samples. It causes the Nitrogen-BET measurement unit to be lower than the Fe_2O_3/SiO_2 catalyst than the unit area of the empty SiO_2 support area oxidized at high temperature, and Fe_2O_3 deposition occurs on the SiO_2 surface [40].

Analysis of the Properties and Characteristics of SiO_2 and Fe_2O_3

Silicon dioxide (SiO_2) is the most plentiful constituent of the layer and has several polymorphs. Underneath environmental conditions, every chemical element atom in silicon oxide is encircled by four O_2 atoms [58]. In 1961 silicon-oxide could be a porous solid. This porous structure is said to the extent the smaller the silicon oxide pore size leads to the larger extent so that the surface assimilation ability will increase. Additionally, silicon oxide has distinctive properties that are not owned by alternative inorganic compounds, like inert properties, sensible surface assimilation, and natural process properties, straightforward to switch with high chemical compounds, and may be used for preconcentration or separation of analytes as a result of the method of binding the analyte to the silicon oxide surface is natural. Reversible. Silicon oxide created from rice husks has many blessings compared to mineral silicon oxide. Wherever rice husk silicon oxide has finer grains, is additional reactive, will be obtained simply at a comparatively low price and is supported by the supply of plentiful and renewable raw materials [59].

Iron sand is ore within the type of sand usually found in nature mixed with sand. Iron sand contains iron minerals with a reasonably high concentration. Iron sand is created thanks to the erosion of natural rocks that contain iron minerals, which happens thanks to the method of destruction by weather and rain that then accumulates and is washed away by waves of brine or watercourse water. River flow. The content of magnetic minerals in iron sands like magnetic iron-ore (Fe_3O_4), iron ore (α-Fe_2O_3), and maghemite (γ-Fe_2O_3) open opportunities to be utilized or developed as industrial raw materials [60]. Table 6 Shows some of the properties of SiO_2 and Fe_2O_3 materials in various material applications.

Research [66] explained that the metal-silica gel chemical agent would absorb the substrate. The surface assimilation of alkoxyl radicals to colloid fertilized with Na metal will bring the substrate and negatron donor nearer. The employment of colloid as support additionally will increase each substrate's effective extent and ambit and, therefore, the metal within the pores

to decrease the activation entropy for negatron transfer. Isomers with internal steric resistance can modify additional thermodynamically stable conformers [67].

Table 6. Review of the properties of SiO_2 and Fe_2O_3 materials in various material applications.

No	Materials	Characteristic	Value of research results	Ref.
1.	Me_2- CA-BTP/SiO_2-P	Have good absorption ability	It was stated that Me_2-CA-BTP/SiO_2-P showed efficient adsorption selectivity towards 241Am(III) above 152Eu(III) in a wide range of nitric acid and acceptable adsorption kinetics work for adequate stability against irradiation in HNO_3 solution. 1 and 3 M, thus successfully separating 241Am(III) from the simulated 3 M HNO_3 HLLW. More specifically, taking into account the overall efficient performance of the adsorbent Me_2-CA-BTP/SiO_2-P, which has great application potential to separate MA directly from HLLW, and is expected to form a modern and simplified MA separation process, which is very meaningful for nuclear energy development.	[61]
2.	SiO_2f/SiO_2, as a silica ceramic matrix composite	High thermal shock resistance, excellent ablation resistance, and low thermal conductivity	The test results from the FEA and brazing equipment produced high-quality E-SiO_2f/SiO_2-Nb joints and the shear strength reached 61.9 MPa.	[62]
3.	Conductive SiO_2 Nanoparticles	Good electrical conductivity due to heterogeneous incorporation of (N, C, and Cl) atoms on the surface of SiO_2 nanoparticles	Their study said that SiO_2 nanoparticles are conductive to doped microwaves and have very efficient microwave absorption. A large microwave reflection loss (RL) of 55.09 dB. The enormous absorption of microwaves comes from electrical relaxation to magnetic relaxation of the incoming microwave field.	[63]
4.	Silica nanosol (SiO_2) on rubber wood	Can improve mechanical properties and thermal stability	The hygroscopicity of the modified wood is reduced, and the dimensional stability is improved. Possibly, the hardness level of the ISB specimen increased by 43.65%. Measurements using thermogravimetry (TG) showed that the incorporation of silicon slowed thermal decomposition and increased the thermal stability of the wood.	[64]
5.	Type-N α-Fe_2O_3 Semikonduktor	Effective light absorption, massive extent, distinctive surface properties, and power stability.	Results from DRIFT for nanocomposites show the active chemical conversion kinetics of the redox catalytic effect in CO_2 reduction and ethanol oxidation. After that, evaluation of the photoelectrochemical CO_2 reduction performance of the nanocomposite was obtained employing linear sweep voltammetry (LSV), and the results showed a significant increase in initial potential (–0.58 V) for the RGO (30 wt %) -SiO_2@α -Fe_2O_3 nanocomposite.	[65]

Another study describes the optimization of the optical absorption of mixture nanoparticles SiO_2@Au and Fe_3O_4@Au. Colloids with their distinctive optical properties can be transformative agents for several applications, notably medicine applications, wherever they'll activate unprecedentedly increased multimodal biosensing, bioimaging, and therapeutic functions. Within the analysis applied, it was found that the particle size and incident wavelength ranged from five to a hundred nm and 600-1200 nm, severally. Therefore, the shell thickness ranged from zero to 100 percent of the particle radius. The analysis additionally

showed that the SiO_2@Au mixture showed several sharp absorption peaks from the Fe_3O_4 @Au mixture. It can be thanks to the loss of core Fe_3O_4, which contributes considerably to the absorption [66]. The expansion of SiO_2 on the water's surface at low temperatures is greatly expedited if the O_2 molecules area unit excited [68].

One crystalline half shows the formation of both diffractograms, verifiable through the physical phenomenon peaks characteristic for Fe_3O_4 at intervals the Fd-3m three-dimensional crystal system and associated Miller index. For both, the presence of an amorphous phase at an angle of 2θ of 20–25° are going to be attributed to the silicon oxide layer within the nanoparticle what is more, by scrutiny the two samples; it'll be same that the microwave-assisted hydrothermal methodology is expounded to successive share of silicon oxide within the sample, as a result of the physical phenomenon phase within the sample magnetite silica SW incorporates a better intensity. Consequently, the crystallinity of this sample is reduced due to the intensity of the physical phenomenon peaks for sample magnetite silica CP is slightly exaggerated, shown in Figure 1. a [69].

The crystallite size for both samples was calculated using the Debye–Scherrer equation:

$$FWHM = \frac{K\lambda}{D\cos\theta'} \quad (1)$$

where FWHM is the full width at the half peak height, K is the Scherrer constant that varies between 0.89 and 0.94, λ is the X-ray wavelength, D is the crystallite size, and θ is the diffraction angle [69]. In this manner, the average crystallite size calculated as the mean value between all peaks is presented in Table 7. As expected, the crystallite size for the nanoparticles obtained through the hydrothermal method is larger due to the crystal growth under increased pressure and temperature conditions. Moreover, the crystallite size of the nanosystems is considerably smaller than other results available in the scientific literature [69].

Table 7. The crystallite size values for the Fe_3O_4@SiO_2_CP and Fe_3O_4@SiO_2_SW samples were calculated using the diffractograms' information.

Sample	description	D Average (nm)	Reference
Fe_3O_4@SiO_2_CP	Co-precipitation (CP)	9.31	[69]
Fe_3O_4@SiO_2_SW	Synth-wave (SW)	11.16	

Figure 1. b The magnetization curve shows that the particles obtained have superparamagnetic characteristics. The saturation magnetization value of each sample is 59 emu g^{-1} for Fe_3O_4, 35 emu g^{-1} for Fe_3O_4/SiO_2, and 17 emu g^{-1} for $Fe_3O_4/SiO_2/TiO_2$. Their results showed that the saturation magnetization decreased with SiO_2 and TiO_2 layers. However, the addition can eliminate particles from the suspension and the external magnetic flux. At a temperature of 150°C, the synthesized sample showed the best saturation magnetization value and will be tested in other photocatalytic experiments [70].

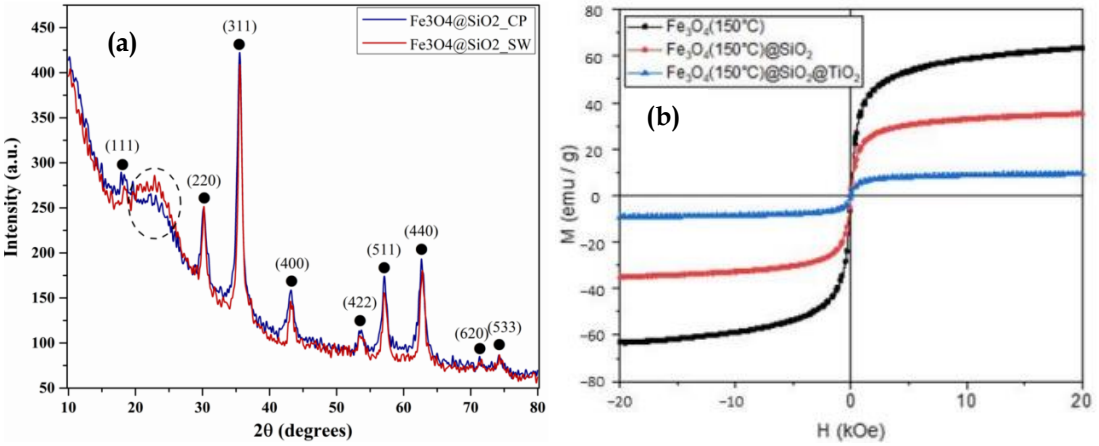

Figure 1. (a) Characteristic XRD sample Fe_3O_4@SiO_2 samples (• —Fe_3O_4) [69], (b) Magnetization curves of Fe_3O_4, Fe_3O_4/SiO_2, and Fe_3O_4/SiO_2/TiO_2 nanoparticles synthesized by the microwave-assisted methodology at 150°C [70] reuse and permission from MDPI.

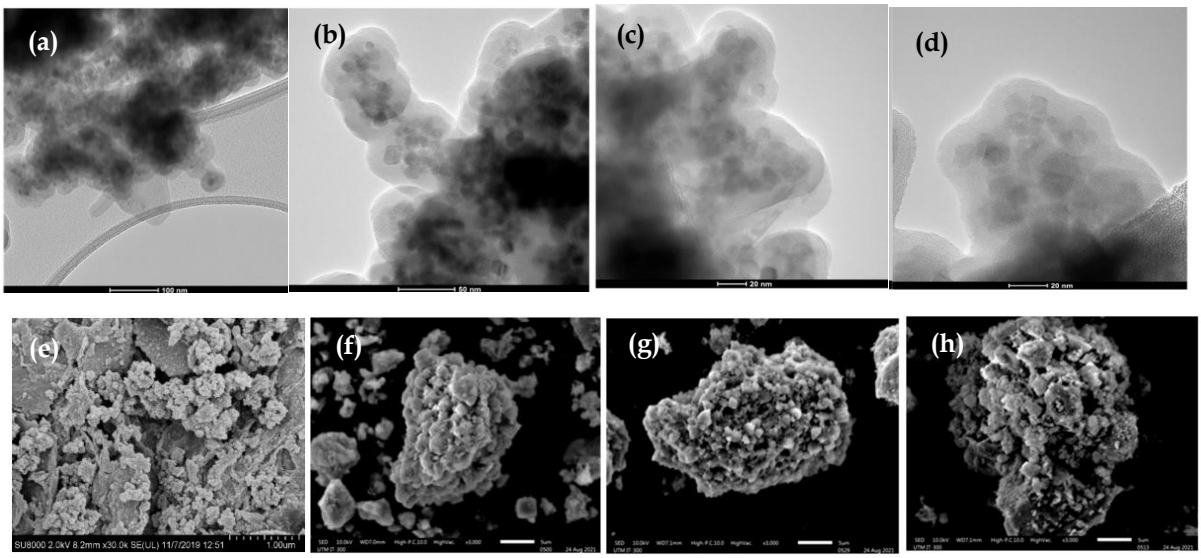

Figure 2. (a-d) Characteristic TEM sample Fe_3O_4@SiO_2 with synthesis core-shell [69], Characteristic SEM sample (e) fresh, (f) reused, (g) ultrasonic, and (h) with microwave CRL/SiO_2/Fe_3O_4/GO (3000× magnification) [71] reuse and permission from MDPI.

From Figure 2. (a-d), it can be seen that the sample groups of 1 to 10 nanoparticles surrounded by a layer of silica have a thick surface. Then, their TEM characterization results were used to confirm the core nanoparticle size and the shell layer thickness. The measured number of shell layers corresponds to the ImageJ computer code pattern. It is supported by the data obtained. a suitable size distribution is created, and the pattern is fitted according to the Gaussian image form obtained in the Original computer code [69]. In addition, the TEM images show the spherical shape of the magnetite nanoparticles. In this context, previous studies have reported the subcubic shape of the nanoparticles retained after silica coating, which is associated with the increased chemical stability afforded by silica coating. Therefore, it can be assumed that the current Fe_3O_4@SiO_2 core-shell nanoparticles have a long service life due to SiO_2 components [69].

Figure 2. e shows the results of the characterization of SEM CRL/SiO_2/Fe_3O_4/GO., which shows immobilization of CRL on the surface of GL-A-SiO_2/Fe_3O_4/GO and producing a very dense exterior of the CRL/SiO_2/Fe_3O_4/GO accelerator. Their results showed that the sample was decorated with white granules with irregular shapes, which was not CRL. Figure 2. f-g depicts reused SEM imaging with microwave regeneration. After eleven cycles, the external acceleration morphology showed varying deposits and a fragmented surface, indicating that the CRL active site blockade occurred. In stark contrast to the freshly prepared and collectively determined CRL/SiO2/Fe3O4/GO morphologies, mechanical-related damage. The residue was presumed to be from a non-free substrate or an enzymatically synthesized unit of measurement; the new substrate was shunted into the active site of CRL/SiO_2/Fe_3O_4/GO. It indicates a reduction in the proportion of warmth units (≈48%) with further use of the accelerator [71]. Post-ultrasonic (Fig. 2g) and microwave processing (Fig. 2h) on the CRL/SiO_2/Fe_3O_4/GO surface appeared to be reduced, indicating that the obstruction at the active catalyst site was less. The effect of the treatment on the CRL/SiO_2/Fe_3O_4/GO samples was extraordinarily effective, with a high heat synthesis temperature of 150% to reach the best at temperatures of 70.51% and 81.68%, respectively [71].

Advanced Application of SiO_2 and Fe_2O_3 Materials

Water pollution has emerged jointly of the foremost serious environmental problems worldwide. Utilizing Fe_2O_3 modified using TiO by modifying the surface layer by atomic layer deposition (ALD) with an ultra-thin layer [51] demonstrated a strong route for application in building efficient and stable photocatalysts. The efficiency of photocatalytic degradation is inversely proportional to the initial concentration of chloramine and directly proportional to the photocatalyst dose. In addition to using the modification of TiO to Fe_2O_3, the application of photocatalysts can be made with Single-atom catalysts (SACs) by utilizing the synthesis method of SiO and Fe, showing excellent performance on protons in the exchange of fuel cells against membranes, and showing great potential to be used as more practical application [72]. Apart from being a material that can overcome water pollution in the environment, several other applications of SIO_2 and Fe_2O_3 can also be useful in everyday life as shown in Table 8. We would like to inform you that this material is very attractive and functional with various benefits.

Table 8. Further applications of SiO_2 and Fe_2O_3 materials

Materials	Synthesis method	Application	Value of research results	Ref.
Fe_2O_3/TiO_2 heterojunction	Layer by atomic layer deposition (ALD)	Photocatalysis	The results showed that the photocatalytic activity of visible light was very good for Modified Fe_2O_3 treated with TiO_2 powder. Four hundred cycles of Fe_2O_3-coated TiO_2 photocatalyst (~2.6 nm) showed excellent degradation efficiency of 97.4% in 90 minutes, different from pure TiO_2 powder, which was only 12.5%.	[51]
Stearic acid (SA) with SiO_2 shell	Sol-gel	Energy Storage	Based on the analysis of thermal properties, the SATEOS6 apparatus shows very promising capabilities as a heat energy storage with melting and solidification temperatures at 70.37°C and 64.27°C and the latent heat of fusion with solidification of 182.53 J/g and 160.12 J / g, respectively. The maximum encapsulation efficiency was found at 86.68% for SATEOS6.	[73]

Fe_3O_4@SiO_2/Pd 0/PdII Nanocomposite	Solution chemicals standard Schlenk techniques	Tandem Suzuki clutch/transfer hydrogenation reaction	The mixed five valence nanocatalyst offers easy magnetic separation and repeated use for multiple cycles. Catalyst exhibiting tandem reactivity together with smooth separation capability.	[74]
Chemical mechanical planarization (CMP) Silicon dioxide	Wet-precipitation AFM and FFM.	Thin Film - SiO_2	The best CMP performance with minimum abrasive zeta potential (~13 mV) and abrasive secondary size (~130-nm size) can be achieved at a certain CMP slurry pH (6.0) which is different from the synthesis termination pH (5.0). Characteristics The pH-sensitive of the superfine abrasive-based SiO_2-film CMP slurry enabled the study of the stability of the CMP slurry. In addition, further chemical design studies to achieve low Cost (i.e., the dependence of solid loading on CMP performance) and CMP self-stop function (i.e., polishing rate selectivity between SiO_2-, Si3N4-, and poly-Si-film) are of great importance. For various CMP applications in nanoscale semiconductor devices.	[75] [76]
Au-PDA@SiO_2/rGO /GCE	StÖber	Electrochemical Sensor	Innovative modified Au-PDA@SiO_2/rGO/GCE electrode for sensitive CEF detection. The proposed sensor can measure the target analyte at very low concentrations with a detection limit of 1.0×10-10 M. Compared to other CEF sensors, the modified electrode exhibits a wide linear range long term stability. Therefore, this electrochemical sensor can successfully determine CEF in pharmaceutical preparations.	[77]
SiO_2 nanofiber filter	The Vapour Liquid-Solid (VLS)	Malaria Diagnosis :fluorescent blue-ray	The automated system demonstrated higher sensitivity (100%) and specificity (92.8%) for detecting Plasmodium falciparum from the blood of 274 asymptomatic individuals in Kenya when compared to the general rapid diagnosis test (sensitivity = 98.1% and specificity = 54, 8%)	[78]
Au@SiO_2 nanoparticles		Transport electron	Unprecedented long-distance transport across one, even three layers of Au@SiO_2 at the junction, with a cumulative isolation gap (silica) until the 29nm/NP layer is reached, far beyond the limit. Measured for standard quantum mechanical tunneling across the insulator (~2.5nm at 0.5-1V). These findings open up a new interdisciplinary field of exploration in nanoelectronics with broad potential impact in fields such as electronic information transfer.	[79]
SiO_2–MgO nanopartikel multiwalled carbon nanotubes (MWCNT)	Sol-gel	Polymer composite	The results show that the physical bond of the polymer has changed and increased its brittleness. These observations indicate that the MWCNT dispersion increases in the polymer matrix. It verifies our proposition that different types of fillers have different effects on mechanical properties	[80]
SiO_2 nanocubes	Two-step hard-template growth	Lithium-ion batteries	The crosslinked polymer gel composite electrolyte effectively encapsulates the electrolyte solution without solvent leakage and exhibits favorable interfacial characteristics. In place of chemical crosslinking, using mesoporous SiO_2 nanoparticles	[22]

			was more effective than non-porous SiO_2 nanoparticles to obtain good cycling performance in release capacity, retention capacity, rate capability, and high-temperature cycling stability.	
$Mn_3[Co(CN)_6]^2$@ SiO_2 Core-shell Nanocubes		MRI and optical imaging	The core-shell Cube nano can offer high-resolution cell fluorescence imaging with two-photon excitation (720 nm) or conventional fluorescence with 403- or 488-nm excitation.	[81]
CuO@SiO_2	HTC two-step method	Catalyst/photocatalyst	Hollow CuO@SiO_2 spheres with an average diameter of 240 nm and a thin shell about 30 nm thick were synthesized using an inorganic SiO_2 coating on the surface of the Cu@C composite obtained by the hydrothermal method. Two stages.	[82]
Ag@SiO_2 Nanoparticles		Sensor metal-enhanced fluorescent (MEF)	The experiment was completed within 30 min with a detection limit of 0.33 nM at the interference of high ether metal concentrations. The sensor was applied to detect Hg^{2+} do in water samples which obtained recovery of more than 91%	[83]
SiO_2/Eu nanoparticles	Sol-gel	Sensor luminescent	Coating the surface of SiO_2 with Eu ions, SiO_2 nanoparticles (20 ~ 50 nm) were immersed in 50 mM $EuCl_3$ ethanol solution at 70 'C for 30 minutes so that the Eu ions on SiO_2 were coated on the surface (this material is from now on referred to as SiO_2/Eu)	[84]

The adsorption application has several advantages technologically simple (simple equipment) and adaptable to many treatment formats, Wide range of commercial products, Wide variety of target contaminants (adsorption). But on the other hand, there are disadvantages such as Relatively high investment, Cost of materials, Nondestructive processes, Non-selective methods Performance depends on the type of material. While the silica gel application has several advantages Highly effective process (adsorption) with fast kinetics, Excellent quality of the treated effluent, Global Elimination but possibly selective depending on the adsorbent, Excellent ability to separate a wide range of pollutants, in particular, refractory molecules (CAC is the most effective material), CAC: efficient for chemical oxygen demand removal; highly efficient treatment when coupled to coagulation to reduce suspended solids, chemical oxygen demand, and color Sand: efficient for turbidity and suspended solids removal, Alumina: efficient for fluoride removal. But on the other hand, there are disadvantages such as a Requirement for several types of adsorbents, Chemical derivatization to improve their adsorption capacity, Rapid saturation, and clogging of the reactors (re-generation-costly), Not efficiency with certain types of dyestuffs and some metals. The elimination of the adsorbent (requires incineration, regeneration, or replacement of the material), Regeneration is expensive and results in loss of material, Economically non-viable for certain industries (pulp and paper, textile, etc.) [85].

Conclusion

Based on our review, we conclude that the hydrothermal method has advantages over other methods such as relatively low-cost, non-toxicity, environmentally friendly precursors, and simple procedures. The benefits of combining SiO_2 with Fe_2O_3, silica, and iron sand/magnetite material attracted our attention because of their easy synthesis and can be quickly processed from natural materials found in nature. A characterization that has to be done is XRD, TEM, SEM, and VSM. XRD to examine the crystal structure of the sample, TEM offers valuable data regarding the structure among the sample, like crystal structure, morphology, and stress state

data. In contrast, SEM provides data regarding the sample surface and its composition and VSM to see the magnetism of a fabric. Seeing the ability of SiO_2 and Fe_2O_3 materials that can be applied as adsorption, catalysis, and further filtration materials, these materials have great potential in overcoming water pollution in the environment. We hope that in the future, there will be a lot of integration of laboratory research that develops the extraordinary materials of silica and magnetite in dealing with water pollution in the environment.

Acknowledgment

The research/publication of this text was funded by DIPA of Public agency of Universitas Sriwijaya 2021. SP DIPA-023.17.2.677515 /2021, on November 23, 2020. Following the Rector's Decree Number: 0010/ UN9/ SK.LP2M.PT/2021, on April 28, 2021.

References

[1] A. Issakhov, A. Alimbek, and Y. Zhandaulet, "The assessment of water pollution by chemical reaction products from the activities of industrial facilities: Numerical study," *J. Clean. Prod.*, vol. 282, p. 125239, 2021.

[2] M. C. Villarín and S. Merel, "Paradigm shifts and current challenges in wastewater management," *J. Hazard. Mater.*, vol. 390, no. January, p. 122139, 2020.

[3] A. Izadi, A. Mohebbi, M. Amiri, and N. Izadi, "Removal of iron ions from industrial copper raffinate and electrowinning electrolyte solutions by chemical precipitation and ion exchange," *Miner. Eng.*, vol. 113, pp. 23–35, 2017.

[4] C. Zamora-Ledezma *et al.*, "Heavy metal water pollution: A fresh look about hazards, novel and conventional remediation methods," *Environ. Technol. Innov.*, vol. 22, p. 101504, 2021.

[5] S. Wacławek, H. V. Lutze, K. Grübel, V. V. T. Padil, M. Černík, and D. D. Dionysiou, "Chemistry of persulfates in water and wastewater treatment: A review," *Chem. Eng. J.*, vol. 330, pp. 44–62, 2017.

[6] S. Giri, "Water quality prospective in Twenty-First Century: Status of water quality in major river basins, contemporary strategies, and impediments: A review," *Environ. Pollut.*, vol. 271, p. 116332, 2021.

[7] I. Saikia, M. Hazarika, N. Hussian, M. R. Das, and C. Tamuly, "Biogenic synthesis of Fe2O3@SiO2 nanoparticles for ipso-hydroxylation of boronic acid in the water," *Tetrahedron Lett.*, vol. 58, no. 45, pp. 4255–4259, 2017.

[8] W. S. Chai *et al.*, "A review on conventional and novel materials towards heavy metal adsorption in wastewater treatment application," *J. Clean. Prod.*, vol. 296, p. 126589, 2021.

[9] Q. Feng *et al.*, "Synthesis of high specific surface area silica aerogel from rice husk ash via ambient pressure drying," *Colloids Surfaces A Physicochem. Eng. Asp.*, vol. 539, no. December 2017, pp. 399–406, 2018.

[10] W. Li *et al.*, "Experimental study on shear property and rheological characteristic of superfine cement grouts with nano-SiO2 addition," *Constr. Build. Mater.*, vol. 228, 2019.

[11] M. Kavand, P. Eslami, and L. Razeh, "The adsorption of cadmium and lead ions from the synthesis wastewater with the activated carbon: Optimization of the single and binary systems," *J. Water Process Eng.*, vol. 34, no. January, p. 101151, 2020.

[12] J. L. Marques *et al.*, "Removal of Al (III) and Fe (III) from binary system and industrial effluent using chitosan films," *Int. J. Biol. Macromol.*, vol. 120, no. Iii, pp. 1667–1673, 2018.

[13] V. P. Dinh *et al.*, "Insight into the adsorption mechanisms of methylene blue and chromium(III) from aqueous solution onto pomelo fruit peel," *RSC Adv.*, vol. 9, no. 44, pp. 25847–25860, 2019.

[14] Y. Wei *et al.*, "Fast and efficient removal of As(III) from water by CuFe2O4 with peroxymonosulfate: Effects of oxidation and adsorption," *Water Res.*, vol. 150, no. Iii, pp. 182–190, 2019.

[15] D. Bouazza, H. Miloudi, M. Adjdir, A. Tayeb, and A. Boos, "Competitive adsorption of Cu (II) and Zn (II) on impregnate raw Algerian bentonite and efficiency of extraction," *Appl. Clay Sci.*, vol. 151, no. November 2017, pp. 118–123, 2018.

[16] S. Narzary, K. Alamelu, V. Raja, and B. M. Jaffar Ali, "Visible light active, magnetically retrievable Fe3O4@SiO2@g-C3N4/TiO2 nanocomposite as efficient photocatalyst for removal of dye pollutants," *J. Environ. Chem. Eng.*, vol. 8, no. 5, p. 104373, 2020.

[17] S. Rohilla *et al.*, "Excellent UV-Light Triggered Photocatalytic Performance of ZnO . SiO 2 Nanocomposite for Water Pollutant Compound Methyl Orange Dye," *nanomaterials*, vol. 11, no. 2548, pp. 1–17, 2021.

[18] P. Sharma, J. Kherb, J. Prakash, and R. Kaushal, "A novel and facile green synthesis of SiO2 nanoparticles for removal of toxic water pollutants," *Appl. Nanosci.*, no. 0123456789, 2021.

[19] H. R. Ali, H. N. Nassar, and N. S. El-Gendy, "Green synthesis of α-Fe2O3 using Citrus reticulum peels extract and water decontamination from different organic pollutants," *Energy Sources, Part A Recover. Util. Environ. Eff.*, vol. 39, no. 13, pp. 1425–1434, 2017.

[20] H. H. Mungondori, S. Ramujana, D. M. Katwire, and R. T. Taziwa, "Synthesis of a novel visible light responsive γ-Fe 2 O 3 /SiO 2 / C-TiO 2 magnetic nanocomposite for water treatment," *Water Sci. Technol.*, vol. 78, no. 12, pp. 2500–2510, 2018.

[21] J. Wang *et al.*, "SiO2 mediated templating synthesis of γ-Fe2O3/MnO2 as peroxymonosulfate activator for enhanced phenol degradation dominated by singlet oxygen," *Appl. Surf. Sci.*, vol. 560, no. May, p. 149984, 2021.

[22] N. Yan *et al.*, "Hollow Porous SiO2 nanocubes towards high-performance anodes for lithium-ion batteries," *Sci. Rep.*, vol. 3, pp. 1–6, 2013.

[23] L. Hao, H. Song, L. Zhang, X. Wan, Y. Tang, and Y. Lv, "SiO 2/graphene composite for highly selective adsorption of Pb(II) ion," *J. Colloid Interface Sci.*, vol. 369, no. 1, pp. 381–387, 2012.

[24] M. Khan and I. M. C. Lo, "Removal of ionizable aromatic pollutants from contaminated water using nano γ-Fe 2 O 3 based magnetic cationic hydrogel: Sorptive performance, magnetic separation and reusability," *J. Hazard. Mater.*, vol. 322, pp. 195–204, 2017.

[25] S. Teixeira *et al.*, "Photocatalytic degradation of recalcitrant micropollutants by reusable Fe3O4/SiO2/TiO2 particles," *J. Photochem. Photobiol. A Chem.*, vol. 345, pp. 27–35, 2017.

[26] M. Rincón Joya, J. Barba Ortega, J. O. D. Malafatti, and E. C. Paris, "Evaluation of

Photocatalytic Activity in Water Pollutants and Cytotoxic Response of α-Fe2O3 Nanoparticles," *ACS Omega*, vol. 4, no. 17, pp. 17477–17486, 2019.

[27] X. L. Chen, F. Li, H. Y. Chen, H. J. Wang, and G. G. Li, "Fe2O3/TiO2 functionalized biochar as a heterogeneous catalyst for dyes degradation in water under Fenton processes," *J. Environ. Chem. Eng.*, vol. 8, no. 4, p. 103905, 2020.

[28] H. A. Budiarti, R. N. Puspitasari, A. M. Hatta, Sekartedjo, and D. D. Risanti, "Synthesis and Characterization of TiO2@SiO2 and SiO2@TiO2 Core-Shell Structure Using Lapindo Mud Extract via Sol-Gel Method," *Procedia Eng.*, vol. 170, pp. 65–71, 2017.

[29] Y. Orooji, S. Mortazavi-Derazkola, S. M. Ghoreishi, M. Amiri, and M. Salavati-Niasari, "Mesopourous Fe3O4@SiO2-hydroxyapatite nanocomposite: Green sonochemical synthesis using strawberry fruit extract as a capping agent, characterization and their application in sulfasalazine delivery and cytotoxicity," *J. Hazard. Mater.*, vol. 400, no. June, p. 123140, 2020.

[30] I. Fatimah *et al.*, "Physicochemical characteristics and photocatalytic performance of TiO2/SiO2 catalyst synthesized using biogenic silica from bamboo leaves," *Heliyon*, vol. 5, no. 11, p. e02766, 2019.

[31] J. Saini, V. K. Garg, and R. K. Gupta, "Green synthesized SiO2@OPW nanocomposites for enhanced Lead (II) removal from water," *Arab. J. Chem.*, vol. 13, no. 1, pp. 2496–2507, 2020.

[32] T. H. Sani, M. Hadjmohammadi, and M. H. Fatemi, "Extraction and determination of flavonoids in fruit juices and vegetables using Fe3O4/SiO2 magnetic nanoparticles modified with mixed hemi/ad-micelle cetyltrimethylammonium bromide and high performance liquid chromatography," *J. Sep. Sci.*, vol. 43, no. 7, pp. 1224–1231, 2020.

[33] D. Asmi, A. Z. Syahrial, and M. Badaruddin, "Improvement High Purity Biogenic Amorphous SiO2 Derived from Rice Husk Ash: Synthesis and its Characterization," *Mater. Sci. Forum*, vol. 1029, pp. 175–180, 2021.

[34] M. Sajjadi, M. Nasrollahzadeh, and S. Mohammad Sajadi, "Green synthesis of Ag/Fe3O4 nanocomposite using Euphorbia peplus Linn leaf extract and evaluation of its catalytic activity," *J. Colloid Interface Sci.*, vol. 497, pp. 1–13, 2017.

[35] E. C. Nnadozie and P. A. Ajibade, "Green synthesis and characterization of magnetite (Fe3O4) nanoparticles using Chromolaena odorata root extract for smart nanocomposite," *Mater. Lett.*, vol. 263, p. 127145, 2020.

[36] X. Weng, L. Ma, M. Guo, Y. Su, R. Dharmarajan, and Z. Chen, "Removal of doxorubicin hydrochloride using Fe3O4 nanoparticles synthesized by euphorbia cochinchinensis extract," *Chem. Eng. J.*, vol. 353, no. May, pp. 482–489, 2018.

[37] R. Heydari, M. F. Koudehi, and S. M. Pourmortazavi, "Antibacterial Activity of Fe3O4/Cu Nanocomposite: Green Synthesis Using Carum carvi L. Seeds Aqueous Extract," *ChemistrySelect*, vol. 4, no. 2, pp. 531–535, 2019.

[38] R. Mahajan, S. Suriyanarayanan, and I. A. Nicholls, "Improved solvothermal synthesis of γ-Fe2O3 magnetic nanoparticles for SiO2 coating," *Nanomaterials*, vol. 11, no. 8, 2021.

[39] Hongbo Yu *et al.*, "One-pot synthesis of Au-Fe2O3@SiO2 core-shell nanoreactors for CO oxidation," *New J. Chem.*, vol. 44, no. 15, pp. 5661–5665, 2020.

[40] A. Nadar *et al.*, "Immobilization of crystalline Fe2O3 nanoparticles over SiO2 for creating an active and stable catalyst: A demand for high temperature sulfuric acid decomposition," *Appl. Catal. B Environ.*, vol. 283, no. October 2020, p. 119610, 2021.

[41] M. Khoshnam and H. Salimijazi, "Synthesis and characterization of magnetic-photocatalytic Fe3O4/SiO2/a-Fe2O3 nano core-shell," *Surfaces and Interfaces*, vol. 26, no. May 2020, p. 101322, 2021.

[42] C. Park, J. Jung, C. W. Lee, and J. Cho, "Synthesis of Mesoporous α-Fe 2 O 3 Nanoparticles by Non-ionic Soft Template and Their Applications to Heavy Oil Upgrading," *Sci. Rep.*, vol. 6, no. August, pp. 1–9, 2016.

[43] X. Ji, W. Zhang, L. Shan, Y. Tian, and J. Liu, "Self-assembly preparation of SiO2@Ni-Al layered double hydroxide composites and their enhanced electrorheological characteristics," *Sci. Rep.*, vol. 5, no. December, pp. 1–10, 2015.

[44] F. Wang *et al.*, "Corn-like, recoverable γ-Fe2O3@SiO2@TiO2 photocatalyst induced by magnetic dipole interactions," *Sci. Rep.*, vol. 7, no. 1, pp. 2–11, 2017.

[45] G. Bharath, S. Anwer, R. V. Mangalaraja, E. Alhseinat, F. Banat, and N. Ponpandian, "Sunlight-Induced photochemical synthesis of Au nanodots on α-Fe2O3@Reduced graphene oxide nanocomposite and their enhanced heterogeneous catalytic properties," *Sci. Rep.*, vol. 8, no. 1, pp. 1–14, 2018.

[46] M. R. A. Kumar, B. Abebe, H. P. Nagaswarupa, H. C. A. Murthy, C. R. Ravikumar, and F. K. Sabir, "Enhanced photocatalytic and electrochemical performance of TiO2-Fe2O3 nanocomposite: Its applications in dye decolorization and as supercapacitors," *Sci. Rep.*, vol. 10, no. 1, pp. 1–15, 2020.

[47] Y. Xu *et al.*, "A hydrophobic FeMn@Si catalyst increases olefins from syngas by suppressing C1 by-products," *Science (80-.).*, vol. 613, no. February, pp. 610–613, 2021.

[48] B. T. da Fonseca, E. D'Elia, J. M. Siqueira Júnior, S. M. de Oliveira, K. L. dos Santos Castro, and E. S. Ribeiro, "Study of the characteristics and properties of the SiO2/TiO2/Nb2O5 material obtained by the sol–gel process," *Sci. Rep.*, vol. 11, no. 1, pp. 1–15, 2021.

[49] P. Ning, X. Song, K. Li, C. Wang, L. Tang, and X. Sun, "Catalytic hydrolysis of carbonyl sulphide and carbon disulphide over Fe2O3 cluster: Competitive adsorption and reaction mechanism," *Sci. Rep.*, vol. 7, no. 1, pp. 2–10, 2017.

[50] C. Li *et al.*, "Hierarchical hollow Fe2O3 @MIL-101(Fe)/C derived from metal-organic frameworks for superior sodium storage," *Sci. Rep.*, vol. 6, no. January, pp. 1–8, 2016.

[51] Y. Q. Cao *et al.*, "Enhanced visible light photocatalytic activity of Fe2O3 modified TiO2 prepared by atomic layer deposition," *Sci. Rep.*, vol. 10, no. 1, pp. 1–10, 2020.

[52] S. Bahadorikhalili, L. Ma'mani, H. Lijan, and M. Mahdavi, "γ-Fe2O3@SiO2(CH2)3-HPBM-Pd as a versatile boosted nanocatalyst for carboncarbon bond f[sbnd]ormation," *Mater. Today Commun.*, vol. 26, no. July, 2021.

[53] J. Edianta, N. Fauzi, M. Naibaho, F. S. Arsyad, and I. Royani, "Review of the effectiveness of plant media extracts in barium hexaferrite magnets (Bafe12o19)," *Sci. Technol. Indones.*, vol. 6, no. 2, pp. 39–52, 2021.

[54] S. Gholamrezaei, M. Salavati-Niasari, D. Ghanbari, and S. Bagheri, "Hydrothermal preparation of silver telluride nanostructures and photocatalytic investigation in degradation of toxic dyes," *Sci. Rep.*, vol. 6, no. October 2015, pp. 1–13, 2016.

[55] M. Le Pivert, R. Poupart, M. Capochichi-Gnambodoe, N. Martin, and Y. Leprince-Wang, "Direct growth of ZnO nanowires on civil engineering materials: smart materials for supported photodegradation," *Microsystems Nanoeng.*, vol. 5, no. 1, pp. 1–7, 2019.

[56] Y. Ma, Y. Wang, T. Jiang, F. Zhang, X. Li, and Y. Zhu, "Hydrothermal synthesis of novel 1-aminoperylene diimide/TiO2/MoS2 composite with enhanced photocatalytic activity," *Sci. Rep.*, vol. 10, no. 1, pp. 1–15, 2020.

[57] O. V. Makarchuk, T. A. Dontsova, and I. M. Astrelin, "Magnetic Nanocomposites as Efficient Sorption Materials for Removing Dyes from Aqueous Solutions," *Nanoscale Res. Lett.*, vol. 11, no. 1, 2016.

[58] M. Misawa *et al.*, "Picosecond amorphization of SiO2 stishovite under tension," *Sci. Adv.*, vol. 3, no. 5, pp. 1–8, 2017.

[59] G. F. Agung M, M. R. Hanafie Sy, and P. Mardina, "Ekstraksi Silika Dari Abu Sekam Padi Dengan Pelarut Koh," *Konversi*, vol. 2, no. 1, p. 28, 2013.

[60] Rizki Kusuma, "Analisis Struktur Kristal Dan Sifat Magnetik Pasir Besi Sungai Bengawan Solo Kecamatan Trucuk Kabupaten Bojonegoro," 2017.

[61] S. Y. Ning *et al.*, "Direct separation of minor actinides from high level liquid waste by Me 2 -CA-BTP/SiO2-P adsorbent," *Sci. Rep.*, vol. 7, no. 1, pp. 1–7, 2017.

[62] Q. Ma *et al.*, "The relation between residual stress, interfacial structure and the joint property in the SiO2f/SiO2-Nb joints," *Sci. Rep.*, vol. 7, no. 1, pp. 1–11, 2017.

[63] M. Green *et al.*, "Doped, conductive SiO2 nanoparticles for large microwave absorption," *Light Sci. Appl.*, vol. 7, no. 1, 2018.

[64] N. Zhang, M. Xu, and L. Cai, "Improvement of mechanical, humidity resistance and thermal properties of heat-treated rubber wood by impregnation of SiO2 precursor," *Sci. Rep.*, vol. 9, no. 1, pp. 1–9, 2019.

[65] U. Kasimayan *et al.*, "In-situ DRIFT investigation of photocatalytic reduction and oxidation properties of SiO2@α-Fe2O3 core-shell decorated RGO nanocomposite," *Sci. Rep.*, vol. 10, no. 1, pp. 1–13, 2020.

[66] X. Xue, V. Sukhotskiy, and E. P. Furlani, "Optimization of Optical Absorption of Colloids of SiO2@Au and Fe3O4@Au Nanoparticles with Constraints," *Sci. Rep.*, vol. 6, no. October, pp. 1–10, 2016.

[67] M. Kapoor and J. R. Hwu, "Na@SiO2-Mediated Addition of Organohalides to Carbonyl Compounds for the Formation of Alcohols and Epoxides," *Sci. Rep.*, vol. 6, no. October, pp. 6–13, 2016.

[68] S. Gurbán *et al.*, "Electron irradiation induced amorphous SiO2 formation at metal oxide/Si interface at room temperature; Electron beam writing on interfaces," *Sci. Rep.*, vol. 8, no. 1, pp. 1–7, 2018.

[69] B. S. Vasile, C. Chircov, M. Matei, and I. A. Neacs, "Iron Oxide – Silica Core – Shell Nanoparticles Functionalized with Essential Oils for Antimicrobial Therapies," pp. 1–26, 2021.

[70] I. Gabelica, L.' Curkovi'c, V. Mandi'c, I. Panži'c, D. Ljubas, and K. Zadro, "Rapid Microwave-Assisted Synthesis of Fe3O4/SiO2/TiO2 Core-2-Layer-Shell Nanocomposite for Photocatalytic Degradation of Ciprofloxaci," pp. 4–5, 2019.

[71] A. G. Jacob, R. A. Wahab, and Mailin Misson, "Operational Stability, Regenerability, and Thermodynamics Studies on Biogenic Silica/Magnetite/Graphene Oxide Nanocomposite-Activated Candida rugosa Lipase," 2021.

[72] L. Jiao *et al.*, "Nanocasting SiO2 into metal–organic frameworks imparts dual protection to high-loading Fe single-atom electrocatalysts," *Nat. Commun.*, vol. 11, no. 1, pp. 1–7, 2020.

[73] S. Ishak, S. Mandal, H. S. Lee, and J. K. Singh, "Microencapsulation of stearic acid with SiO2 shell as phase change material for potential energy storage," *Sci. Rep.*, vol. 10, no. 1, pp. 1–15, 2020.

[74] P. Singh, S. Mishra, A. Sahoo, and S. Patra, "A magnetically retrievable mixed-valent Fe3O4@SiO2/Pd0/PdII nanocomposite exhibiting facile tandem Suzuki coupling/transfer hydrogenation reaction," *Sci. Rep.*, vol. 11, no. 1, pp. 1–11, 2021.

[75] Y. H. Son *et al.*, "Super fine cerium hydroxide abrasives for SiO2 film chemical mechanical planarization performing scratch free," *Sci. Rep.*, vol. 11, no. 1, pp. 1–10, 2021.

[76] R. I. Revilla, X. J. Li, Y. L. Yang, and C. Wang, "Large electric field-enhanced-hardness effect in a SiO2 film," *Sci. Rep.*, vol. 4, 2014.

[77] M. Z. H. Khan, M. Daizy, C. Tarafder, and X. Liu, "Au-PDA@SiO2 core-shell nanospheres decorated rGO modified electrode for electrochemical sensing of cefotaxime," *Sci. Rep.*, vol. 9, no. 1, pp. 1–6, 2019.

[78] T. Yamamoto *et al.*, "Development of a quantitative, portable, and automated fluorescent blue-ray device-based malaria diagnostic equipment with an on-disc SiO2 nanofiber filter," *Sci. Rep.*, vol. 10, no. 1, pp. 1–12, 2020.

[79] C. Li, C. Xu, D. Cahen, and Y. Jin, "Unprecedented efficient electron transport across Au nanoparticles with up to 25-nm insulating SiO2-shells," *Sci. Rep.*, vol. 9, no. 1, pp. 1–9, 2019.

[80] K. Nemeth *et al.*, "Synthesis and investigation of SiO2-MgO coated MWCNTs and their potential application," *Sci. Rep.*, vol. 9, no. 1, pp. 1–11, 2019.

[81] Y. Huang *et al.*, "Mn3[Co(CN)6]2@SiO2 Core-shell Nanocubes: Novel bimodal contrast agents for MRI and optical imaging," *Sci. Rep.*, vol. 3, pp. 1–7, 2013.

[82] X. Niu, T. Zhao, F. Yuan, and Y. Zhu, "Preparation of hollow CuO@SiO2 spheres and its catalytic performances for the NO + CO and CO oxidation," *Sci. Rep.*, vol. 5, no. 1, pp. 1–8, 2015.

[83] Y. Pang, Z. Rong, R. Xiao, and S. Wang, " 'turn on' and label-free core - Shell Ag@SiO2 nanoparticles-based metal-enhanced fluorescent (MEF) aptasensor for Hg2+," *Sci. Rep.*, vol. 5, pp. 1–8, 2015.

[84] A. Ishii and M. Hasegawa, "An interfacial europium complex on SiO2 nanoparticles: Reduction-induced blue emission system," *Sci. Rep.*, vol. 5, pp. 5–10, 2015.

[85] G. Crini and E. Lichtfouse, "Advantages and disadvantages of techniques used for wastewater treatment," *Environ. Chem. Lett.*, vol. 17, no. 1, pp. 145–155, 2019.